Nanoparticulate $Ni(OH)_2$ Films Synthesized from Macrocyclic Nickel(II) Cyclam for Hydrogen Production in Microbial Electrolysis Cells

Mohan Qin,[a,=] William A. Maza,[b,=] Bethany M. Stratakes,[b] Spencer R. Ahrenholtz,[b] Amanda J. Morris,[b,*,z] and Zhen He[a,*,z]

[a]*Department of Civil and Environmental Engineering, Virginia Polytechnic Institute and State University, Blacksburg, Virginia 24061, USA*
[b]*Department of Chemistry, Virginia Polytechnic Institute and State University, Blacksburg, Virginia 24061, USA*

Hydrogen production in microbial electrolysis cells (MECs) is a promising approach for energy harvesting from wastewater. The kinetic barriers toward proton reduction necessitate the use of catalysts to drive hydrogen formation at appreciable rates and low applied potentials. Towards this end, cost effective alternatives to platinum catalysts are of paramount interest. In this study, $Ni(OH)_2$ films were synthesized by electrophoretic deposition from a Ni(II)cyclam precursor solution at varying concentrations (6 mM, 15 mM, and 23 mM). The films were characterized by scanning electron microscopy and X-ray photo-electron spectroscopy to confirm the deposition of $Ni(OH)_2$. The $Ni(OH)_2$-modified electrodes were then examined by both traditional electrochemical measurements and in an MEC for hydrogen production. Tafel analysis indicates an exchange current density of ~0.36 mA cm^{-2} with a Tafel slope of ~120 mV $decade^{-1}$ consistent with a rate determining proton adsoprtion step. The hydrogen production rates increased with increasing Ni(II)cyclam concentration in the precursor solution, with the 23 mM-derived film exhibiting a rate comparable to that of a Pt-based catalyst in MEC tests.
 [DOI: 10.1149/2.1081605jes] All rights reserved.

Manuscript submitted November 17, 2015; revised manuscript received February 1, 2016. Published February 19, 2016.

Hydrogen is considered to be one of the most promising energy carriers as an alternative fuel because of its high energy density and availability from renewable sources. Over 90% of hydrogen gas is produced by steam reforming and coal gasification, both of which are highly energy-consuming processes.[1] Among the newly developed technologies for hydrogen production, microbial electrolysis cells (MECs) are of special interest as a new approach for hydrogen production from organic matter in wastewater and other organic waste.[2,3] In an MEC, organic compounds are degraded by exoelectrogens (electrochemically-active microorganisms), and as a result, electrons are passed to an anode electrode. Hydrogen gas can be formed at the cathode (−0.414 V vs. SHE, standard hydrogen electrode) by reducing protons. This process must be aided by an additional voltage (0.114 V in theory) as a result of the insufficiency of the anode potential (e.g., −0.300 V vs. SHE when acetate is used as an anode substrate) to drive proton reduction. In reality, an external voltage of more than 0.2 V is required to overcome the additional kinetic barriers imposed by the hydrogen formation reaction.[4] This additional voltage is substantially lower than that needed for electrochemical water splitting (theoretically 1.23 V vs. SHE[5]) making hydrogen production energetically more cost efficient. In addition, recovery of valuable energy content from wastewater/waste also results in environmental benefits.

Catalysts are indispensable in accomplishing the hydrogen evolution reaction (HER). Most MEC studies have used platinum-based catalysts for HER catalysis. Platinum is a highly efficient catalyst for HER, but its high cost obstructs its application in MECs, especially for large scale systems that are designed for wastewater treatment.[4,6] Thus, alternative catalysts have been explored such as Pd-,[7] Fe-,[8] Mo-,[9] and Ni-based materials.[10] Among them, Ni-containing nanoparticles are of special interest because of nickel's low cost, abundance, low overpotentials toward proton reduction, and high stability in solutions, which are usually alkaline in the MEC cathode.[4,11] For example, a cathode catalyst was developed by electrodepositing NiMo onto a three-dimensional carbon-fiber-weaved cloth material, and at an applied voltage of 0.6 V, the MECs achieved a hydrogen production rate of 0.09 m^3 m^{-2} d^{-1} (m^3 H_2 per m^2 cathode surface area per day) at a sustained current density of 12 A m^{-2} (A per m^2 cathode surface area).[12] The rate of hydrogen production by the NiMo-modified carbon cloth was comparable to that of a Pt-modified carbon cloth (0.10 m^3 m^{-2} d^{-1}). Commercially available nickel was also used as a catalyst coated on carbon cloth for MEC cathodes.[13] Nickel oxide catalysts have also shown great promise as catalysts for hydrogen evolution in MECs.[14] Electrodeposition of nickel oxide onto stainless steel and nickel alloy surfaces have been shown to improve the MEC hydrogen production from 0.0002 m^3 m^{-2} d^{-1} (no Ni oxide) to 0.019 m^3 m^{-2} d^{-1} at a current density of 3.25 A m^{-2} when a 0.9 V external voltage bias was applied.[11]

In this study, a nano-$Ni(OH)_2$ modified cathode was developed by electrodeposition from a nickel(II) cyclam (cyclam = 1, 4, 8, 11-tetraazacyclotetradecane) precursor. The synthetic method was based on a procedure of the deposition of $Ni(OH)_2$ using [Ni(en = ethylene diamine)$_3$]Cl_2, resulting in homogeneous, well adhered $Ni(OH)_2$ thin film.[13,15] The [Ni(en)$_3$]Cl_2-derived $Ni(OH)_2$ films were shown to exhibit significantly higher catalytic activity toward water oxidation than films derived from $[Ni(OH_2)_6]^{2+}$ solutions under similar conditions.[15] The morphology and composition of the films generated here were investigated via scanning electron microscope (SEM) and X-ray photoelectron spectroscopy (XPS). The catalytic activity toward hydrogen production was examined through electrochemical techniques and in an MEC.

Experimental

Materials.—Reagents or analytical grade chemicals were sourced from commercial suppliers and used as received unless stated otherwise. Deionized water was used throughout the study.

Synthesis procedure.—Ni(II)cyclam was prepared by refluxing equimolar nickel(II) chloride hexahydrate (99.3%, Alfa Aesar) and 1,4,8,11-tetraazacyclotetradecane (>95%, Ark Pharm Inc) in dimethylformamide (DMF) (99.8% spectrophotochemical grade, Spectrum) at 90°C for 12 hours. The purple precipitate was filtered and washed with a copious amount of DMF to remove any excess $Ni(II)Cl_2 \cdot 6H_2O$ and then allowed to dry. This method differs slightly from typical synthetic approaches in which equimolar amounts of $Ni(II)Cl_2$ and the tetraazacyclotetradecane are dissolved in methanol

=These authors contributed equally to this work.
*Electrochemical Society Member.
zE-mail: zhenhe@vt.edu; ajmorris@vt.edu

or ethanol and the product separated by addition of ether.[16,17] Our approach affords a precipitated product in nearly quantitative yields.

The $Ni(OH)_x$ films were electrodeposited onto carbon cloth (PANEX 30PW03, Zoltek Corporation, St. Louis, MO, USA) with an area of 4 cm^2 (2 cm × 2 cm) by dissolving the Ni(II)cylcam precursor in a solution of 0.1 M NaOH. The potential was then cycled between 0 V and 1.3 V (vs Ag/AgCl) for 150 cycles. A three electrode arrangement was employed using the carbon cloth as the working electrode, a platinum mesh counter electrode, and an Ag/AgCl (sat. KCl) half-cell as the reference electrode. The electrodeposition was carried out in a one-compartment electrochemical cell under aerobic conditions at room temperature. The procedure employed was similar to that used by Singh, et al. for the deposition of Ni(OH)x films onto glassy carbon electrodes and fluorine doped tin oxide electrodes from $Ni(NH_3)_6$, $Ni(OH_2)_6$, $Ni(en)_3$ (en = 1,2-diaminoethane), and other Ni(II) amine molecular precursors.[15] The nomenclature of nano-scaled $Ni(OH)_2$ represents the nickel hydroxide prepared with X mM Ni(II) cyclam as the precursor where X could be 6, 15, and 23.

Characterization.—LEO (Zeiss) 1550 field emission scanning electron microscope (FESEM) operating at an acceleration voltage of 300 KV was employed to study the morphology and structural properties of the nanoparticulate films. FEI Quanta 600 FEG environmental scanning electron microscope (ESEM) with Bruker energy-dispersive X-ray spectroscopy (EDS) was used to analyze the elemental composition of the catalyst. XPS was conducted using a PHI 5300 spectrometer with a Perkin-Elmer Dual Anode X-ray source operating with monochromatic Mg Kα radiation (hν 1253.6 eV) at 13 kV and 250 W and a pass energy of 17.9 eV. A step size of 0.1 eV was used and 256 sweeps were averaged for all measurements. The photoelectrons emitted were detected by a hemispherical analyzer. Operating pressure in the sampling chamber was below 1×10^{-7} Torr. The spectral range for Ni 2p was 894–844 eV, N 1s was 410–390 eV, and O 1s 545–525 eV. The spectra were calibrated according to the C 1s peak at 284.6 eV.

Electrochemical analysis.—The synthesized catalysts were coated onto a piece of rectangular carbon cloth (PANEX 30PW03, Zoltek Corporation, St. Louis, MO, USA) with an area of 4 cm^2 (2 cm × 2 cm), which was used as a cathode electrode. A cathode coated with 0.5 mg cm^{-2} Pt/C (10% wt Platinum on Carbon Vulcan, Fuel Cell Earth LLC, Wakefield, Ma, USA) was prepared and served as a control.

Tafel plots (scan rate 1 mV s^{-1}) were prepared with chronoamperametric data obtained on a potentiostat (Reference 600, Gamry Instruments, Warminster, PA, USA). Electrochemical experiments were conducted using a three-electrode arrangement in a PBS (1 M, 120 mL) electrolyte solution. The modified cathode electrodes served as a working electrode, a platinum wire served as the counter electrode, and an Ag/AgCl electrode (CH Instruments, Inc., Austin, TX, USA) was used as a reference electrode. The electrochemical cell was sparged with nitrogen gas for 15 min prior to each test.

MEC setup and operation.—A two-chamber MEC (Figure 1) was built by connecting two glass bottles with a cation exchange membrane (CEM) as separator (UltexCMI7000, Membranes International, Inc., GlenRock, NJ, USA), according to a previous study.[9] The liquid volume of the anodic chamber and the cathodic chamber was 130 and 140 mL, respectively. The anode electrode was a carbon brush (Gordon Brush Mfg. Co., Inc., Commerce, CA, USA) which had been cultivated under a microbial fuel cell mode for three months. The anolyte contained (per liter of DI water): sodium acetate (1 g), NaCl (1 g), $MgSO_4$ (0.015 g), $CaCl_2$ (0.02 g), KH_2PO_4 (0.53 g), K_2HPO_4 (1.07 g), $NaHCO_3$ (1 g), and trace element (1 mL).[18] PBS (0.1 M, KH_2PO_4 (5.3 g/L), K_2HPO_4 (10.7 g/L)) solution was used as a catholyte. An external voltage of 0.8 V was applied to the circuit by a power supply (CSI3644A, Circuit Specialists, Inc., Mesa, AZ, USA) according to a previous study.[19] The MEC was operated under a batch mode with an HRT of 30 h. In each cycle, part of the anolyte (60 mL) and the whole catholyte (140 mL) were replaced.

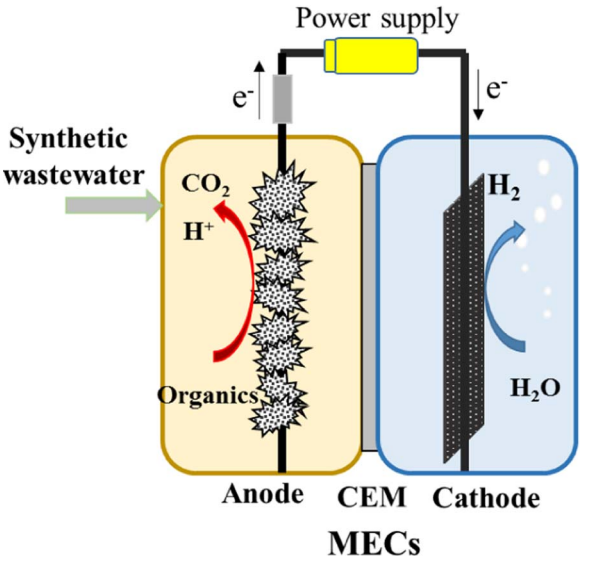

Figure 1. Schematic of an MEC.

The voltage across resistor was recorded with a digital multimeter (2700, Keithley Instruments, Inc., Cleveland, OH, USA) with a time interval of 5 min. Current was calculated by Ohm's law. Hydrogen production in the MEC was collected by water displacement and measured with a syringe. Chemical oxygen demand (COD) was measured with a DR/890 colorimeter (HACH Co., Ltd., USA) according to the manufacturer's instructions. The content of H_2 was analyzed using a Shimadzu GC-14A gas chromatograph equipped with a thermal conductivity detector (TCD).

Calculation.—Coulombic efficiency, cathodic hydrogen recovery, overall hydrogen recovery and hydrogen production rates were used to evaluate reactor performance.[2,8]

The total charge (C_{total}, C) generated by each batch cycle can be calculated based on the measured current:

$$C_{total} = \int I dt \quad [1]$$

where I is the current (A) calculated from the voltage across the resistor (10 Ω) and dt is the time interval (300 s) for data collection.

The Coulombic recovery (C_R) is the ratio of electrons recovered from substrate consumption relative to the total possible electrons available due to substrate consumption, calculated as

$$C_R = \frac{C_{total}}{nF\Delta COD} \quad [2]$$

where n is the number of electrons released from each oxygen (4), F is the Faraday constant (96,485 C mol^{-1} e^-), and ΔCOD is total mole of consumed bacterial feedstock within time t.

The cathodic hydrogen recovery (R_{cat}) is the fraction of electrons that are recovered as hydrogen gas from the total generated electrons:

$$R_{cat} = \frac{2n_{H_2}F}{C_{total}} \quad [3]$$

where n_{H_2} is the actual number of hydrogen moles produced.

The overall hydrogen recovery (R_{H_2}) is the ratio of generated hydrogen gas compared to the theoretical hydrogen generation based on substrate degradation:

$$R_{H_2} = C_R * R_{cat} \quad [4]$$

The hydrogen production rate (Q_{H_2}, m^3 H_2 m^{-2} d^{-1}) is calculated based on the generated hydrogen gas (m^3) per m^2 cathode electrode per day.

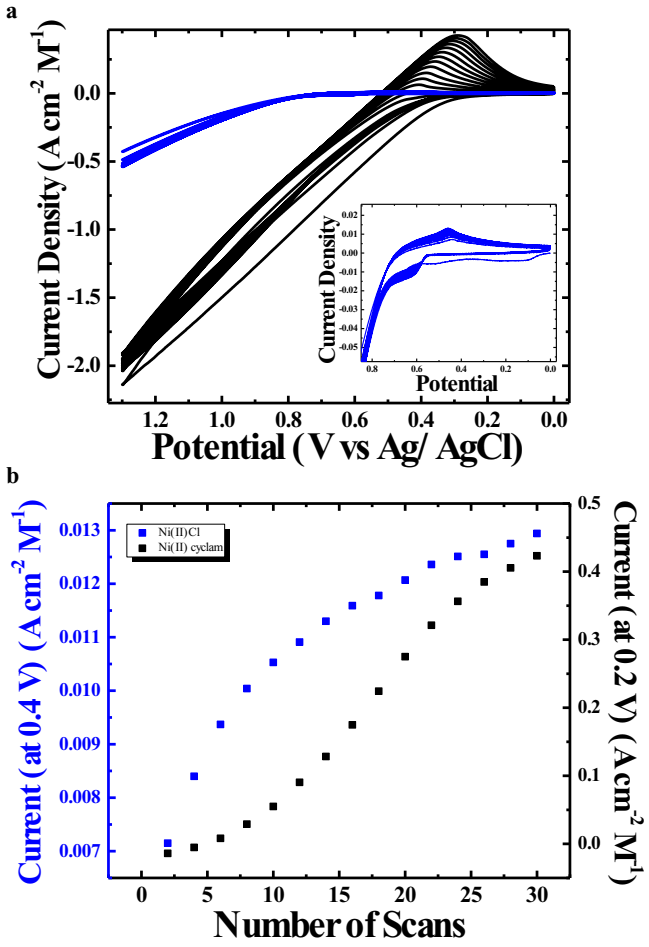

Figure 2. (a) Cyclic voltammograms of Ni(II)cyclam (solid black line) and $Ni(II)Cl_2 \cdot 6H_2O$ in an aqueous 0.1 M NaOH solution. The inset shows a closer view of the $Ni(II)Cl_2 \cdot 6H_2O$ CV. (b) Comparison of the current densities corresponding to the electrodeposition of the Ni(II) catalyst from the Ni(II)cyclam (black) and $Ni(II)Cl_2$ solutions on the CFE as a function of the number of potential sweep scans.

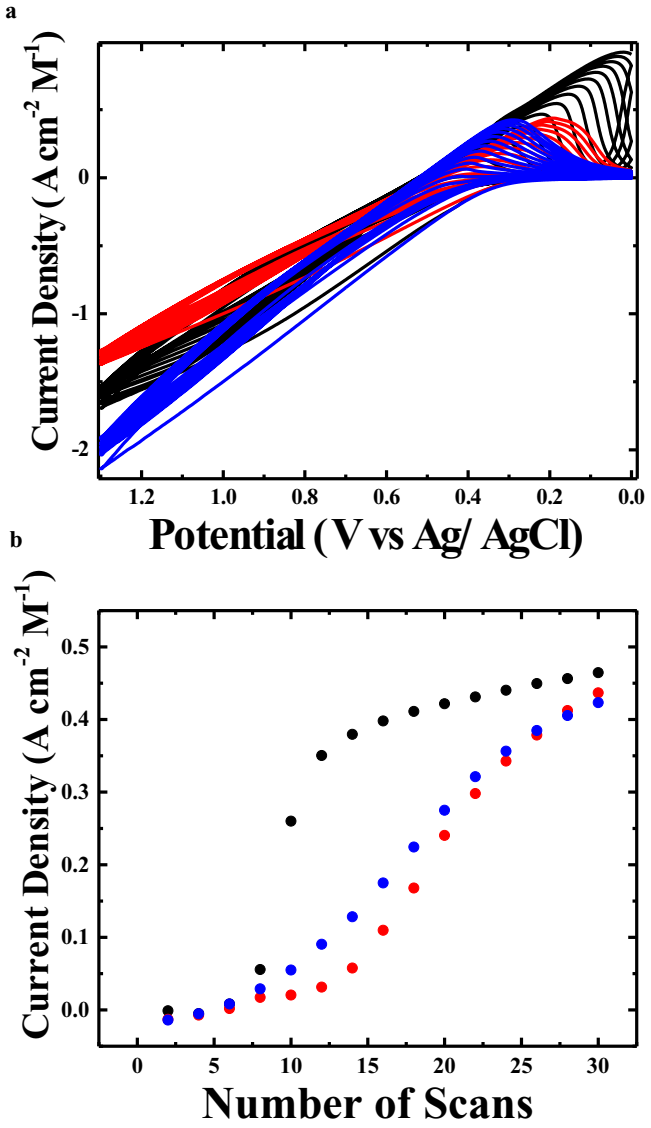

Figure 3. (a) Cyclic voltammograms of 6 mM (solid black line), 15 mM (solid red line), and 23 mM (solid blue line) Ni(II)cyclam solutions in aqueous 0.1 M NaOH electrolyte. (b) Comparison of the current densities corresponding to the electrodeposition of the Ni(II) catalyst from the 6 mmm (black circles), 15 mM (red circles), and 23 mM (blue circles) Ni(II)cyclam solutions on the CFE as a function of the number of potential sweep scans. These are compared to each other by dividing the current densities by the concentration of Ni(II) cyclam at the start of the deposition.

Results and Discussion

Ni(II) catalyst electrodeposition and electrode preparation.— Cyclic voltammograms (CVs) of a carbon felt electrode (CFE) in the presence of 23 mM Ni(II)cyclam in a solution of 0.1 M NaOH are shown in Figure 2a. The CVs display an anodic peak at 410 mV (vs. Ag/AgCl) whose current density increases with increasing potential sweeps. The increase in current density is accompanied by a shift in the anodic peak to more negative potential up to 285 mV. The observed current increase with respect to sweep number is attributed to the deposition of nanoparticulate $Ni(OH)_2$ species. This is consistent with literature reports of $Ni(OH)_2$ deposition from soluble molecular Ni(II) coordination complexes as pre-catalysts on glassy carbon (GCE) as well as fluorine-doped tin oxide (FTO) electrodes in basic borate buffers and NaOH solutions.[15] The $Ni(OH)_2$ has been proposed to form by a Ni—N de-ligation mechanism in the presence of strongly coordinating basic groups.[15]

A plot of the anodic peak current as a function of the sweep number displays a monotonic increase in the concentration current density with a plateau at approximately 420 mA cm^{-2} M^{-1}. Varying the starting solution concentration of Ni(II)cyclam had little effect on the behavior of the concentration-normalized current densities and value of the observed plateau, between 400 mA cm^{-2} M^{-1} and 470 mA cm^{-2} M^{-1} (Figure 3). The steepness of the inflections differ significantly in going from 6 mM Ni(II)cyclam to higher concentrations of Ni(II)cyclam, possibly suggesting a concentration dependent mechanism of film formation.

For comparison, the electrodeposition of $Ni(OH)_2$ films onto CFE from a $Ni(II)Cl_2 \cdot 6H_2O$ solution was also carried out (Figure 2). The CV of $Ni(II)Cl_2 \cdot 6H_2O$ in 0.1 M NaOH displays cathodic and anodic peaks at 520 mV and 440 mV, respectively. Upon continued sweeps the anodic peak potential was observed to shift to slightly more positive potentials reaching a value of 460 mV after 30 sweeps. Much like the electrodeposition from Ni(II)cyclam, nickel hydroxide formation from $Ni(II)Cl_2$ on the surface of the CFE (as evidenced by increasing the anodic peak current density) is monotonic as a function of increasing number of potential sweeps. Due to the poor solubility of $Ni(II)Cl_2 \cdot 6H_2O$ in 0.1 M NaOH the effect of $Ni(II)Cl_2 \cdot 6H_2O$ concentration on $Ni(OH)_2$ formation and deposition could not be probed.

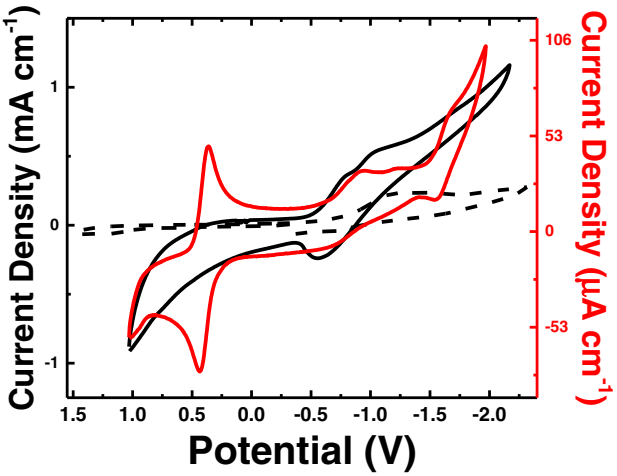

Figure 4. Cyclic voltammograms of a $Ni(OH)_2$ film deposited on CFE (black – left y-axis), carbon cloth (black dash – left y-axis), and Ni(II)cyclam in solution (red – right y-axis, working electrode: glassy carbon) in anaerobic 0.1 M $TBAPF_6$-CH_3CN solutions (scan rate 25 mV/s).

Cyclic voltammetry was performed on the $Ni(OH)_2$ films on CFE and compared to Ni(II)cyclam in anaerobic 0.1 M $TBAPF_6$ solutions in CH_3CN. At a scan rate of 25 mV s^{-1} the CV of the $Ni(OH)_2$ film displays cathodic features at −0.785 V and −1.03 V with an anodic feature at −0.555 V (Figure 4). Similar cathodic features at −0.95 V and −1.22 V with a cathodic feature at −0.68 V were observed in the CV of Ni(II)cyclam at 25 mV s^{-1}. The origin of these features are, as of yet, uncertain. They are, however, consistent with results observed for $Ni(OH)_2$ films deposited from other Ni(II)-amine coordination complexes.[15] Their presence in the $Ni(OH)_2$ films leads us to believe that they may be related to redox activity of $Ni(OH)_2$ adsorbed on the electrode surface that may have formed during polarization.[20] It is important to note that the reversible redox features observed with Ni(II)cyclam with $E_{1/2}$ = 0.398 V and −1.61 V (vs Ag/AgCl) corresponding to the $Ni^{3+/2+}$ and $Ni^{2+/+}$ redox couples, respectively, are not observed in the $Ni(OH)_2$ film.[21–24]

Characterization of the nickel oxide films.—X-ray photoelectron spectroscopy was performed for the films deposited on CFE from 6 mM, 15 mM, and 23 mM Ni(II)cyclam solutions in an attempt to elucidate the nature of the films. The spectra corresponding to the Ni $2p_{3/2}$, N 1s, and O 1s electron binding energies are shown in Figure S1. The Ni $2p_{3/2}$ and O 1s spectra were decomposed by non-linear least squares fitting using Gaussians where the peak positions and FWHM were allowed to vary. The Ni $2p_{3/2}$ and satellite signals for the 23 mM sample film were adequately fit to a single Gaussian each centered at 858.5 eV and 864.3 eV, respectively, whereas the observed O 1s signal was found to be comprised of two underlying Gaussians centered at 532.8 eV and 534.4 eV. The 6 mM and 15 mM samples display similar results with Ni $2p_{3/2}$ (satellite) signals at 858.0 eV (863.9 eV) and 856.2 eV (862.2 eV), as well as O 1s signals at 532.9 eV (with second component at 534.4 eV) and 531.4 eV, respectively.

Based on the data above it is proposed that the films are $Ni(OH)_2$ in nature.[15] XPS signals for $Ni(OH)_2$ are typically 855 eV - 858 eV for the Ni $2p_{3/2}$ and 531 eV for the O 1s binding energies, which are in agreement with the results found here (*vide supra*).[25–27] The cause of the O 1s shift to near 533 eV is uncertain, but may be due to interactions between the $Ni(OH)_2$ nanoparticles and oxygen functional groups on the CFE that may form during the oxidative electrodeposition process under basic conditions. These oxygen functional groups (i.e. carbonyls) on the surface of the CFE may also explain the presence of the second band at 534 eV in the 6 mM and 23 mM preparations.

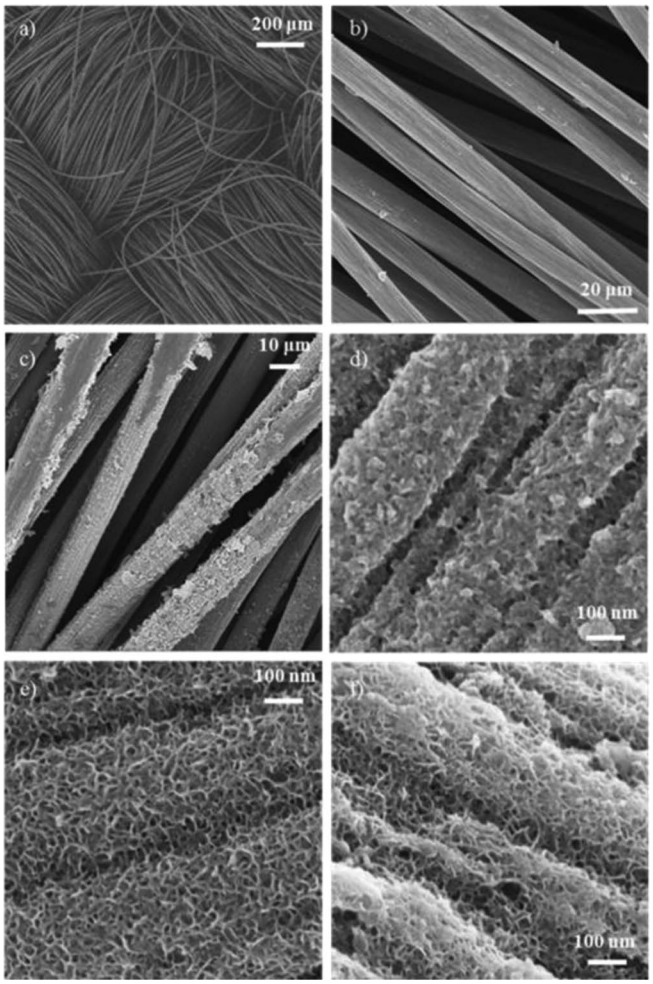

Figure 5. SEM images of carbon cloth (a and b) and $Ni(OH)_2$-modified carbon cloth that results from electrodeposition from a Ni(II)cyclam precursor solution at concentration of 23 mM (c and d), 15 mM (e) and 6 mM (f).

SEM (with EDS) was also employed to characterize the structure of $Ni(OH)_2$ on carbon cloth. Figure 5 shows the FESEM images of $Ni(OH)_2$-coated carbon cloth substrates (Figures 5c–5f). For comparison, FESEM images of the unmodified cloth are also shown (Figures 5a and 5b). The carbon cloth is composed of large interweaved bunches of microfibers with a diameter of ∼15 μm. The figure shows that the surface of unmodified carbon cloth is relatively rough over the size of samples (not all shown here). The SEM images (Figures 5d–5f) indicate the morphology of the $Ni(OH)_2$ nanostructures is comprised of a network of intergrown plates. The irregularity of the orientations of the nano-plates suggest that the films may have large surface areas for reactivity. This could open up new opportunities and applications for catalytic $Ni(OH)_2$-based materials. The $Ni(OH)_2$ film prepared with 23 mM Ni(II)cyclam appeared denser when compared to the films prepared with lower amounts of the precursor material, suggesting the potential of an increased number of catalytic sites when making films with higher amounts of Ni(II)cyclam. Figure S2 presents the ESEM images and EDS spectra of the unmodified carbon cloth and $Ni(OH)_2$ generated from nickel(II) cyclam. All samples displayed EDS peaks corresponding to carbon, resulting from the carbon cloth base. Nickel and oxygen peaks were also present at both sites materials prepared by electrodeposition from nickel(II) cyclam solutions, indicating successful coating of the microfibers. Small amounts of iron were observed in the $Ni(OH)_2$ modified carbon cloth likely due to the contamination during the electrode preparation.

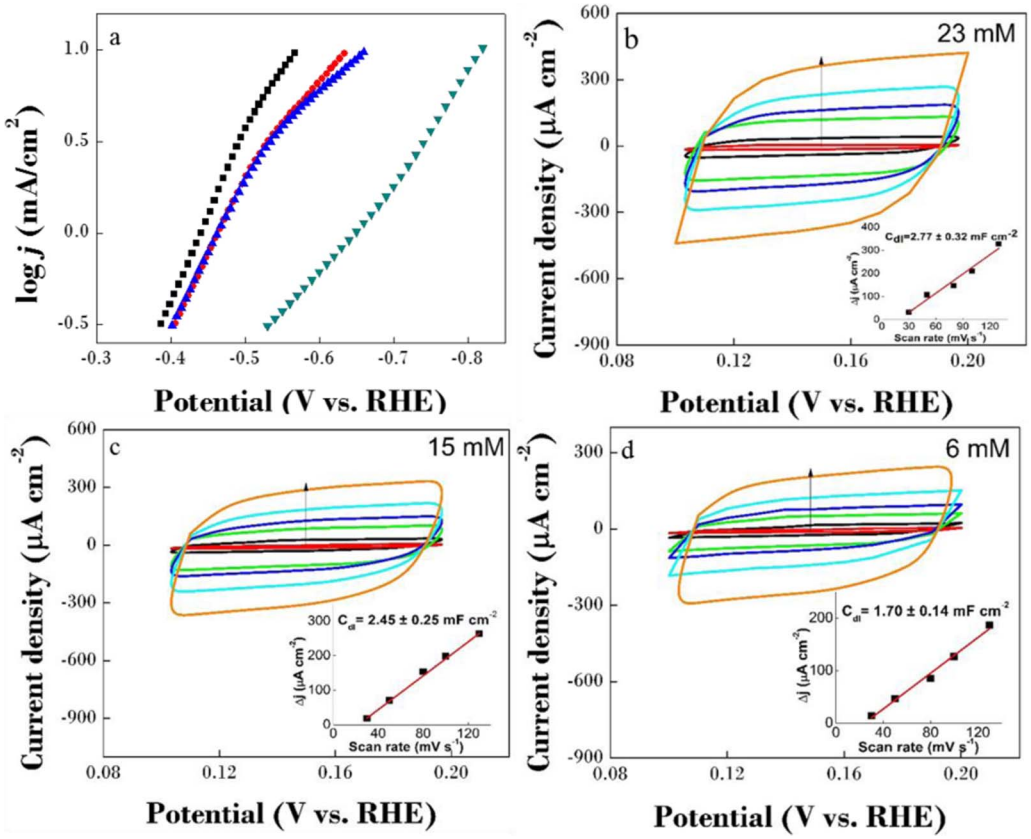

Figure 6. a. Tafel slope for carbon cloth (green), $Ni(OH)_2$ -6 mM precursor (navy), $Ni(OH)_2$ −15 mM precursor (red) and $Ni(OH)_2$ -23 mM precursor (black) with a scan rate of 1 mV s^{-1} measured in PBS buffer (1 M). b-d. CV in the region of 0.1–0.2 V vs. RHE plotted against scan rate and linear regression for the C_{dl} estimation with 23mM, 15 mM and 6 mM Ni(II)cyclam. Scan rate: 130 mV/s (orange), 100 mV/s (blue), 80 mV/s (navy), 50 mV/s (green), 30 mV/s (black), and 10 mV/s (red).

Tafel plots (log (current density) vs overpotential) for unmodified carbon cloth and $Ni(OH)_2$-coated electrodes generated from nickel(II) cyclam were constructed to identify the rate limiting step of hydrogen production (*vida infra*) and are shown in Figure 6. The unmodified electrode exhibits a Tafel slope of 211 mV $decade^{-1}$ and an exchange current of 0.23 mA cm^{-2}. The $Ni(OH)_2$-coated electrodes generated from $Ni(II)Cl_2 \cdot 6H_2O$ showed a Tafel slope of 201 mV $decade^{-1}$. Comparatively, the Tafel analysis of $Ni(OH)_2$-modified electrodes generated from nickel(II) cyclam precursor solutions exhibited Tafel slopes of 105, 123, 129 mV $decade^{-1}$ when the nickel(II) cyclam concentration in the deposition solution were 23, 15, and 6 mM, respectively. The exchange current was 0.34, 0.36, and 0.36 mA cm^{-2}, respectively.

The hydrogen evolution reaction (HER) involves three steps: the Volmer (Eq. 5), Heyrovsky (Eq. 6), and Tafel (Eq. 7) reactions, which involve adsorption of a reduced proton on a surface and chemical recombination to produce H_2 as outlined in Equations 5 to 7.

$$H_3O^+ + e^- \rightarrow H_{ads} + H_2O \quad [5]$$

$$H_{ads} + H_3O^+ + e^- \rightarrow H_2 + H_2O \quad [6]$$

$$2H_{ads} \rightarrow H_2 \quad [7]$$

The expected Tafel slopes for a Volmer, Hyrovsky, or Tafel rate-determining reaction are 120 mV dec^{-1}, 40 mV dec^{-1}, and 30 mV dec^{-1} respectively. Considering the observed Tafel slope of 120 mV $decade^{-1}$, the rate-determining HER step for the $Ni(OH)_2$ films prepared here is most likely the adsorption related reaction (Volmer).

The active catalytic area was estimated through determination of the electrochemical surface area (ECSA) (Figures 6b–6d). The double layer capacitance (C_{dl}), which is expected to be linearly proportional to the effective active surface area, can be determined through investigation of the current response of the $Ni(OH)_2$-modified electrodes in a potential region where no faradaic processes occur. For the $Ni(OH)_2$-modified electrodes, the region of 0.1–0.2 V vs. RHE was used. By plotting the non-faradaic (charging) current vs. scan rate the C_{dl} was quantified. The C_{dl}s for the $Ni(OH)_2$-modified electrodes were determined to be 2.77 ± 0.32 mF cm^{-2}, 2.45 ± 0.25 mF cm^{-2} and 1.70 ± 0.14 mF cm^{-2} for electrodes prepared in 23 mM, 15 mM and 6 mM Ni(II)cyclam precursor solutions, respectively. The ECSA increased as the starting concentration of Ni(II)cyclam in the electrodeposition reaction is increased. Assuming that the C_{dl} is directly proportional to the active surface area, these results strongly suggest that a higher concentration of Ni(II)cyclam precursor results in an increased density of catalytically active sites for hydrogen evolution.

Hydrogen production in an MEC.—Hydrogen generation catalyzed by the developed nano-scale $Ni(OH)_2$ films was investigated in an MEC applying a 0.8 V external voltage. The typical batch-profile current density is shown in Figure 7. In general, the decrease in current density observed with operation time is related to substrate consumption. The results are summarized in Table I. Some salient points arise from the analysis of the MEC experiments. First, it is not surprising that the total charge and Coulombic recovery observed for both the $Ni(OH)_2$ film electrodes (regardless of the method of preparation) and the Pt electrode are within statistical error of each other considering these are dependent on the degree of feedstock consumption by the bacterial anodes.

It is noteworthy, then, that the hydrogen recovery efficiencies, R_{cat}, and overall hydrogen recovery rates, Q_{H2}, for Pt (78.3 ± 1.9% and 0.013 ± 0.001 m^3 H_2 m^{-2} d^{-1}, respectively) and the $Ni(OH)_2$ film

Table I. Hydrogen production and efficiencies of the MECs with modified carbon cloth with nickel hydroxide or Pt and unmodified carbon cloth at an applied voltage of 0.8 V.

		C_{total}[a], C	C_R[b], %	R_{cat}[c], %	R_{H_2}[d], %	Q_{H_2}[e], m^3 H_2 m^{-2} d^{-1}
Ni(II)cyclam	23 mM	71.6 ± 2.1	25.0 ± 3.4	84.3 ± 3.3	20.7 ± 1.1	0.014 ± 0.002
	15 mM	75.5 ± 2.9	27.6 ± 4.7	69.6 ± 4.0	19.2 ± 1.9	0.012 ± 0.003
	6 mM	75.4 ± 2.1	26.4 ± 3.1	59.2 ± 2.1	15.7 ± 1.3	0.010 ± 0.001
$Ni(II)Cl_2 \cdot 6H_2O$		71.1 ± 0.8	22.3 ± 4.0	48.4 ± 4.2	10.8 ± 2.1	0.008 ± 0.002
Pt		71.4 ± 1.2	26.2 ± 2.4	78.3 ± 1.9	19.1 ± 0.9	0.013 ± 0.001
Carbon cloth		40.1 ± 1.0	10.2 ± 1.9	21.1 ± 3.8	2.1± 1.4	0.002 ± 0.001

[a]Total coulombs passed – reports on the complete consumption of the electron source (organics – acetate) in the anode chamber and is expected to be similar for all catalytic cathodes.
[b]Coulombic recovery.
[c]Cathodic hydrogen recovery.
[d]Overall hydrogen recovery.
[e]Hydrogen production rate. All were calculated according to the equation in experimental part.

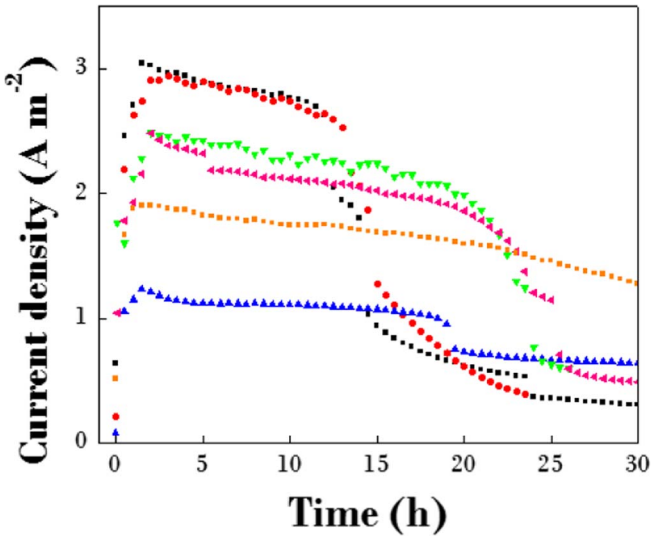

Figure 7. Current density of the MEC with modified carbon cloth with $Ni(OH)_2$ (23 mM Ni(II)cyclam (black), 15 mM (green), and 6 mM (pink)), $Ni(OH)_2$ from $Ni(II)Cl_2 \cdot 6H_2O$ (orange) or Pt (red) and unmodified carbon cloth (blue) at an applied voltage of 0.8 V.

prepared at a higher concentration of Ni(II)cyclam precursor (84.3 ± 3.3% and 0.014 ± 0.002 m^3 H_2 m^{-2} d^{-1}, respectively) are within statistical error. In addition, there is a noticeable difference in the R_{cat} and Q_{H2} between the $Ni(OH)_2$ films prepared using $NiCl_2$ (at saturating concentrations, R_{cat} = 48.4% and Q_{H2} = 0.008 m^3 H_2 m^{-2} d^{-1}) and Ni(II)cyclam at higher, though well below saturating, concentrations (R_{cat} = 84.3% and Q_{H2} = 0.014 m^3 H_2 m^{-2} d^{-1}). The latter results are consistent with a previous study.[11] Finally, there appears to be a linear relationship between the Ni(II)cyclam precursor concentration and the R_{cat} and Q_{H2}, which is likely related to an increase in the number of catalytic sites available with films prepared at higher precursor concentration, as supported by the determination of the ESCA.

In summary, a method of preparing $Ni(OH)_2$ films has been demonstrated here by electrophoretic deposition from Ni(II)cyclam precursor solutions. The films prepared in this manner displayed excellent performance for catalyzing HER for hydrogen production in MECs comparable to Pt. In addition, the MECs employing the $Ni(OH)_2$ catalyst exhibited stable hydrogen production for one month, therefore, making these Ni-based materials stable electrodes in MECs.

Acknowledgments

We thank Stephen McCartney (Virginia Tech) for his assistance with FESEM and ESEM. This work was financially supported by Virginia Tech Institute for Critical Technology and Applied Science (ICTAS).

References

1. S. Manish and R. Banerjee, *Int J Hydrogen Energ*, **33**(1), 279 (2008).
2. B. E. Logan, D. Call, S. Cheng, H. V. Hamelers, T. H. Sleutels, A. W. Jeremiasse, and R. A. Rozendal, *Environ Sci Technol*, **42**(23), 8630 (2008).
3. R. A. Rozendal, H. V. Hamelers, G. J. Euverink, S. J. Metz, and C. J. Buisman, *Int J Hydrogen Energ*, **31**(12), 1632 (2006).
4. A. Kundu, J. N. Sahu, G. Redzwan, and M. Hashim, *Int J Hydrogen Energ*, **38**(4), 1745 (2013).
5. H. Liu, S. Grot, and B. E. Logan, *Environ Sci Technol*, **39**(11), 4317 (2005).
6. B. Tartakovsky, M. F. Manuel, H. Wang, and S. Guiot, *Int J Hydrogen Energ*, **34**(2), 672 (2009).
7. Y. X. Huang, X. W. Liu, X. F. Sun, G. P. Sheng, Y. Y. Zhang, G. M. Yan, S. G. Wang, A. W. Xu, and H. Q. Yu, *Int J Hydrogen Energ*, **36**(4), 2773 (2011).
8. L. Xiao, Z. Wen, S. Ci, J. Chen, and Z. He, *Nano Energy*, **1**(5), 751 (2012).
9. H. Yuan, J. Li, C. Yuan, and Z. He, *ChemElectroChem*, **1**(11), 1828 (2014).
10. M. F. Manuel, V. Neburchilov, H. Wang, S. Guiot, and B. Tartakovsky, *J Power Sources*, **195**(17), 5514 (2010).
11. P. A. Selembo, M. D. Merrill, and B. E. Logan, *J Power Sources*, **190**(2), 271 (2009).
12. H. Hu, Y. Fan, and H. Liu, *Int J Hydrogen Energ*, **34**(20), 8535 (2009).
13. P. A. Selembo, M. D. Merrill, and B. E. Logan, *Int J Hydrogen Energ*, **35**(2), 428 (2010).
14. A. W. Jeremiasse, H. V. Hamelers, M. Saakes, and C. J. Buisman, *Int J Hydrogen Energ*, **35**(23), 12716 (2010).
15. A. Singh, S. L. Y. Chang, R. K. Hocking, U. Bach, and L. Spiccia, *Energ. Environ. Sci.*, **6**(2), 579 (2013).
16. B. Bosnich, M. L. Tobe, and G. A. Webb, *Inorg Chem*, **4**(8), 1109 (1965).
17. N. H. Voelcker, I. Alfonso, and M. R. Ghadiri, *Chembiochem*, **9**(11), 1776 (2008).
18. L. T. Angenent and S. Sung, *Water Res*, **35**(7), 1739 (2001).
19. S. Yossan, L. Xiao, P. Prasertsan, and Z. He, *Int J Hydrogen Energ*, **38**(23), 9619 (2013).
20. Y. C. Ding, J. L. Yuan, and Z. R. Chang, *J Power Sources*, **69**(1-2), 47 (1997).
21. M. Beley, J. P. Collin, R. Ruppert, and J. P. Sauvage, *J Am Chem Soc*, **108**(24), 7461 (1986).
22. O. Zhalko-Titarenko, O. Lazurskii, and V. Pokhodenko, *Theor. Exp. Chem.*, **26**(1), 40 (1990).
23. A. Jarzębińska, P. Rowiński, I. Zawisza, R. Bilewicz, L. Siegfried, and T. Kaden, *Anal Chim Acta*, **396**(1), 1 (1999).
24. M. Zhang, M. T. Zhang, C. Hou, Z. F. Ke, and T. B. Lu, *Angewandte Chemie International Edition*, **53**(48), 13042 (2014).
25. N. S. Mcintyre and M. G. Cook, *Anal Chem*, **47**(13), 2208 (1975).
26. C. E. Dube, B. Workie, S. P. Kounaves, A. Robbat, M. L. Aksu, and G. Davies, *J Electrochem Soc*, **142**(10), 3357 (1995).
27. A. P. Grosvenor, M. C. Biesinger, R. S. Smart, and N. S. McIntyre, *Surf Sci*, **600**(9), 1771 (2006).